Synthesis and characterization of highly organized crystalline rutile nanoparticles by low-temperature dissolution-reprecipitation process

Mohammad Rezaul Karim[a)]
Center of Excellence for Research in Engineering Materials, Advanced Manufacturing Institutes, King Saud University, Riyadh 11421, Kingdom of Saudi Arabia

Mohammad Tauhidul Islam Bhuiyan
Faculty of Engineering, Particle Technology Research Centre, University of Western Ontario, London, Ontario N6A5B8, Canada

Mushtaq Ahmad Dar, Asiful Hossain Seikh, and Muhammad Ali Shar
Center of Excellence for Research in Engineering Materials, Advanced Manufacturing Institutes, King Saud University, Riyadh 11421, Kingdom of Saudi Arabia

Mohammed Badruz Zaman
AB-Biotech Inc., National Research Council of Canada, Ottawa, Ontario K1A 0R6, Canada; and Center of Excellence for Research in Engineering Materials, Advanced Manufacturing Institutes, King Saud University, Riyadh 11421, Kingdom of Saudi Arabia

Chul Jae Lee
School of Chemical Industry, Yeungnam College of Science and Technology, 170 Hyeonchung-ro, Nam-gu, Daegu 705-703, Republic of Korea

Hee Jin Kim
Department of Chemical Engineering, Pohang University of Science and Technology (POSTECH), Pohang, Gyungbuk 790-784, Republic of Korea

Mu Sang Lee
Department of Chemistry, Kyungpook National University, Daegu 702-701, Republic of Korea

(Received 17 November 2014; accepted 1 May 2015)

Rutile nanoparticles have been synthesized by acid hydrolysis of titanium isopropoxide by low-temperature dissolution-reprecipitation process. High-resolution transmission electron micrographs of the rutile colloidal solution show needle-shaped rutile nanoparticles with the dimensions of 10–30 nm in diameter and 100–150 nm in length. X-ray diffraction (XRD) data show the existence of only the rutile polymorph in TiO_2 powder with a crystallite size of 11.3 nm. The dielectric constant of rutile nanoparticles has been found to be 57 at 10 MHz AC frequency and DC conductance as 2.3×10^{-6} S/cm. Transmission electron micrographs and XRD data analysis imply that the rutile crystallites are self-organized in a regular fashion to produce multilayer three-dimensional linear clusters. The clusters have been found to be microporous (average porosity 1.4 nm) with high specific surface area (132.2 m^2/g). At higher concentration, the clusters aggregate to produce interconnected network of star- or flower-like structures. This organized crystalline microporous metal-oxide semiconductor might find various practical applications.

I. INTRODUCTION

Rutile has been found to be potential material for photocatalytic antibacterial activity,[1] gas sensors,[2,3] batteries,[4,5] solar cells,[6,7] capacitors,[8,9] high-*k* gate insulator,[10] and so on due to low cost production, thermal stability, and most importantly for its semiconductive, dielectric behavior. Potential photoluminescence[11,12] and chemiluminescence[13,14] properties of rutile provide the additional advantage toward its diversified applications. Rutile is the most stable one among the TiO_2 polymorphs and also the most abundant one. Rutile nanoparticle finds more attractive applications for controlled morphology and high specific surface area. Among the synthesis methods of rutile nanoparticles, low-temperature synthesis method is very much attractive to the research community due to low production cost, high purity, soft particle aggregation, higher specific surface area, and uniform shape of the nanoparticles.

Contributing Editor: Edson Roberto Leite
[a)]Address all correspondence to this author.
e-mail: mkarim@ksu.edu.sa
DOI: 10.1557/jmr.2015.150

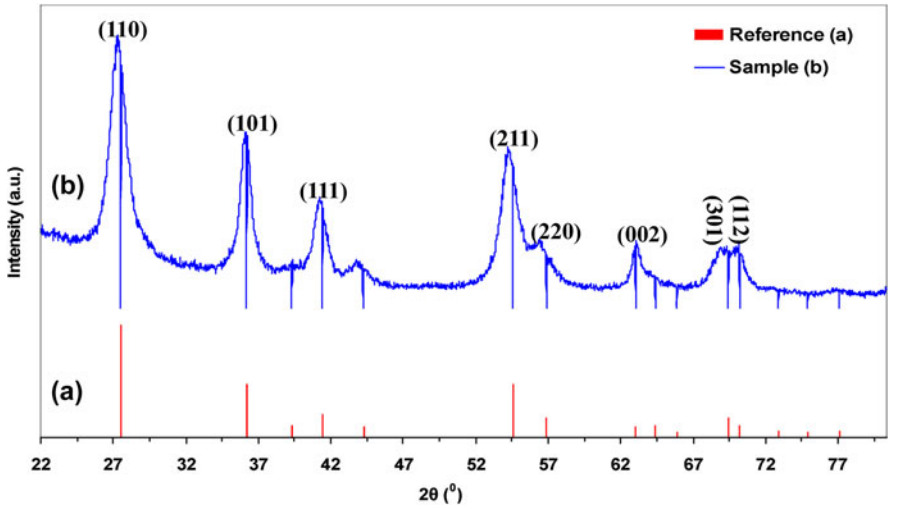

FIG. 1. XRD pattern of rutile nanoparticles: (a) standard reference[20] and (b) synthesized in this work.

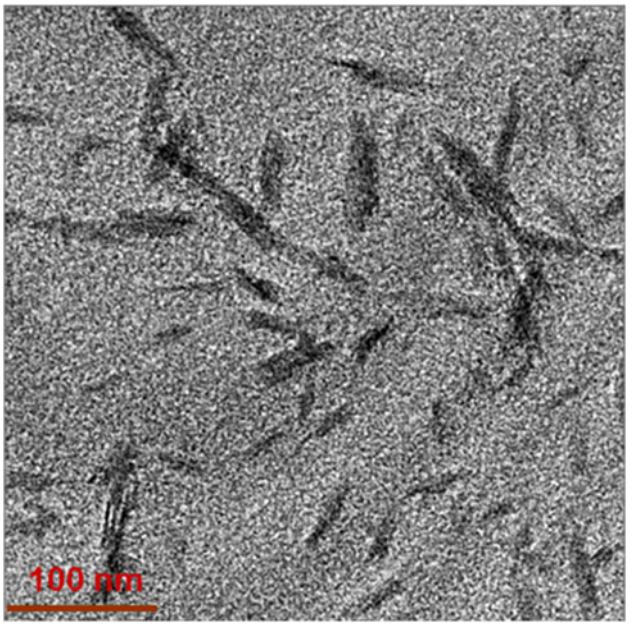

FIG. 2. TEM image of rutile nanoparticles obtained after 4 h of aging.

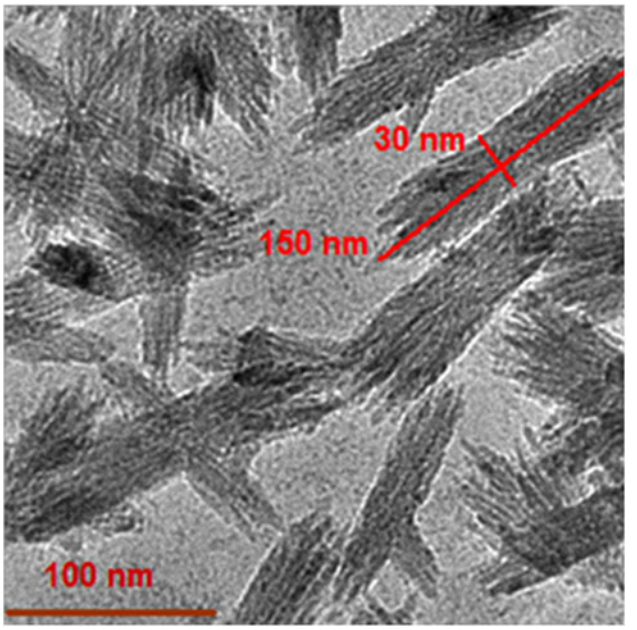

FIG. 3. TEM image of rutile nanoparticles obtained after 72 h of aging.

Several methods have been developed using varying precursors and strategies at reaction temperatures ranging from 20 to 100 °C.[15–17] Previously, all methods were high-temperature methods at the temperature ranging from 130 to 1400 °C.[18,19]

Different methods produce rutile nanoparticles of different morphologies ranging from spherical, oval, rod shape, needle shape, shuttle-like shape to even uneven shape.[15] But highly organized crystalline nanoparticles with uniform porosity at mesoporous to micro level are highly desired materials for various applications. Here, the organized crystalline microporous metal-oxide semiconductor (rutile) nanoparticles synthesized by the low-temperature dissolution-reprecipitation process (LTDRP) has been reported.

II. EXPERIMENTAL SECTION

A. Reagents

All the chemicals used in this experiment are of analytical grade. Titanium tetraisopropoxide (TTIP) and hydrochloric acid have been purchased from Sigma Aldrich.

B. Synthesis of nanoparticles

The organized crystalline microporous metal-oxide semiconductor (rutile) nanoparticles have been synthesized by a modified method of Yin et al.[15] TTIP of 0.005 mol has been added slowly to 18.36 mL water at 24 °C under stirring. White slurry has been produced

instantly. HCl up to 1M acidic concentration has been added to that freshly prepared slurry. Stirring has been continued for 4 h at the same temperature and a clear solution obtained. It has been subjected to aging up to 3 days at 24 °C and white rutile nanoparticles have been obtained.

C. Instruments used

Instruments that have been used here are: a) high-resolution transmission electron microscope (HR-TEM; Philips model CM 200, FEI Company, Eindhoven, Netherlands), b) x-ray diffraction (XRD; Philips model X'Pert APD with a Cu K_α source), c) BET surface area and pore size analyzer (Quantachrome Autosorb-3a; at 77 K by N_2 adsorption after pretreating them at over 300 °C for 1 h to remove adsorbed water), d) Raman spectrometer (Almega X/Thermo), e) elemental analyzer (CE Instruments, model FISON EA-1110), and f) impedance analyzer (HP4291B RF impedance/material analyzer; 1–1.8 GHz).

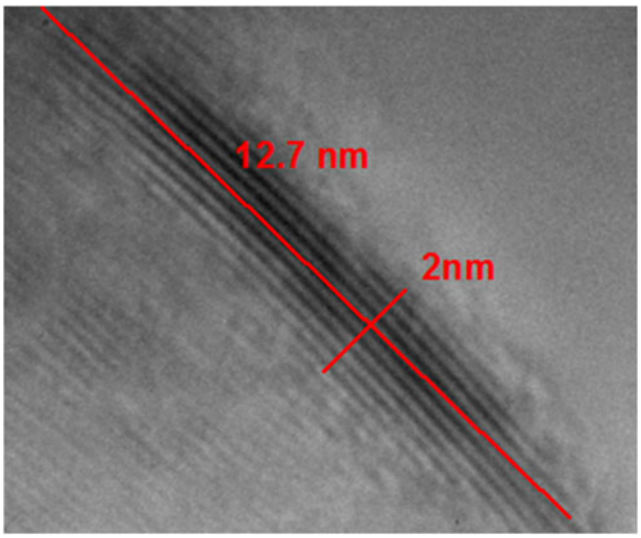

FIG. 4. HR-TEM image of a rutile crystallite after 24 h of aging.

III. RESULTS AND DISCUSSION

A. X-ray diffraction data analysis

The XRD data (Fig. 1) show all the characteristic peaks of rutile completely matched with the standard reference (JCPDS—International Centre for Diffraction Data).[20] This implies that the synthesized TiO_2 nanoparticles are very pure and consist of only rutile polymorph of titania.

The crystallite size of the rutile nanoparticles is calculated by Scherrer's relation[21] (using the 110 face):

$$D = K\lambda/\beta\cos\theta \quad , \tag{1}$$

where $K = 0.89$, D represents the crystallite size (nm), λ is the wave length of Cu K_α radiation, and β is the corrected value at half width of the diffraction peak. This can be attributed to the fact that "crystallite size" is not synonymous with "particle size" while XRD is sensitive to the crystallite size.[22] The characteristic peak of rutile at $2\theta = 27.316°$ has been chosen to calculate the average grain size of rutile nanoparticles and obtained as 11.3 nm.

B. Transmission electron microscopy data analysis

Transmission electron micrographs (TEM) of the rutile nanoparticles show that at the initial stage of aging (e.g., 4 h aged), the particles are not uniform (Fig. 2); but at the longer aging period (e.g., 72 h aged), they are quite uniform with dimensions 25–30 nm in diameter and 130–150 nm in length (Fig. 3). HR-TEM of the rutile nanoparticles (Figs. 4 and 5) shows that the rutile nanoparticles are composed of crystallites in a highly

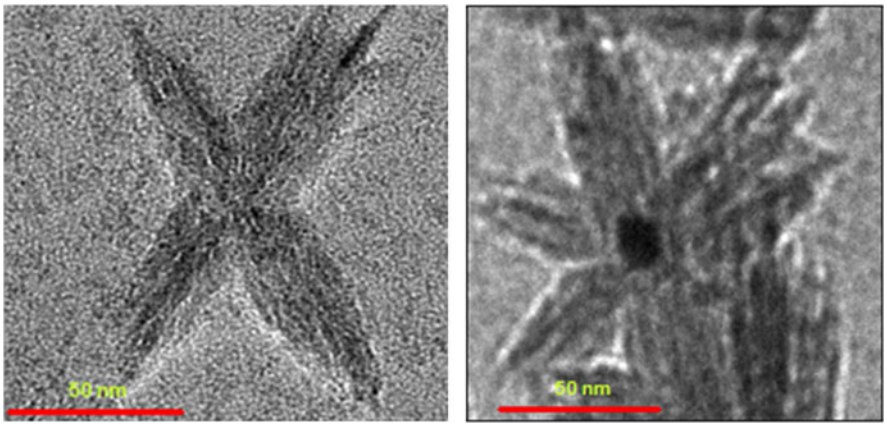

FIG. 5. HR-TEM image of aggregated rutile nanoparticles after 48 h of aging.

organized fashion. The crystallites of the rutile nanoparticles are of dimensions 1.5–2.5 nm in diameter and 10–13 nm in length. Selected area electron diffraction (SAED) image (Fig. 6) of rutile nanoparticles (72 h aged) confirms the crystalline structure of the particles.

C. Surface area and pore size analyzer

The surface area of the rutile nanoparticles (72 h aged) has been determined from the corresponding nitrogen adsorption/desorption isotherms (Fig. 7). The BET surface area of rutile nanopowder is 132.2 m^2/g.

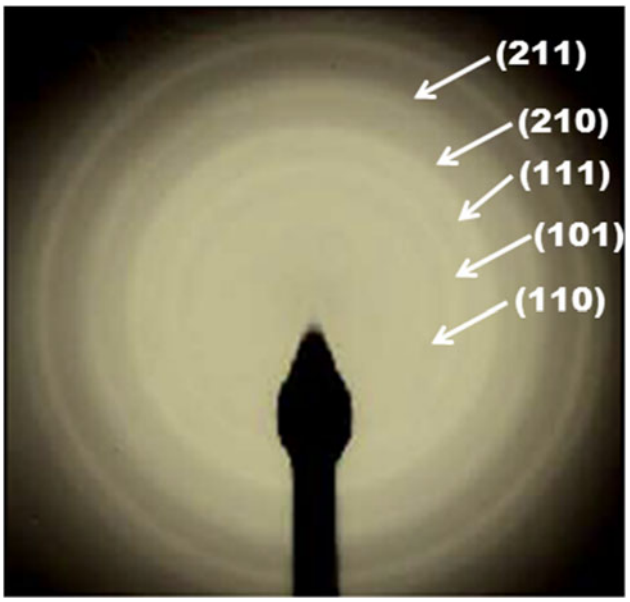

FIG. 6. SAED image of synthesized rutile nanoparticles.

The pore volume and pore size distribution (Fig. 8) are 0.34 cm^3/g and 1.4 nm, respectively, determined using the Barrett–Joyner–Halenda (BJH) model from the data of N_2 isotherms. The pore size distribution analysis of both the samples shows that pore diameters concentrate in the range of 1–10 nm with a high trend in the microporous range which is in good agreement with the HR-TEM observations. The specific surface area and porosity of the rutile nanoparticles have been summarized in Table I.

D. Raman spectra

From Fig. 9, the O–Ti–O network peaks over 400–700 cm^{-1} are characteristics of TiO_2 (72 h aged) in correspondence to the Raman active phonons of rutile 441 cm^{-1} (E_g) and 579 cm^{-1} (A_{1g}).[23,24] The C–H stretching peaks that are clearly evident at around 2900 cm^{-1} confirm the presence of the alkyl groups ($–C_3H_7$) on the surface of rutile nanoparticles. The O–H stretch peak (3000–3700 cm^{-1}) attributes to the large amount of water molecules adsorbed on the surface of the particles and condensed in the pores which is very consistent with the Raman data. This also indicates that the nanoparticles are highly porous.

E. Elemental analysis

The elemental analysis is also proving the presence of $–C_3H_7$ and –OH groups on the rutile nanoparticle surface (72 h aged). Approximately, only 0.08% isopropyl group is present in the sample. Remaining 0.0729% hydrogen quite certainly comes from bound –OH groups and adsorbed water molecules. The elemental analysis data of rutile nanoparticles are given in Table II.

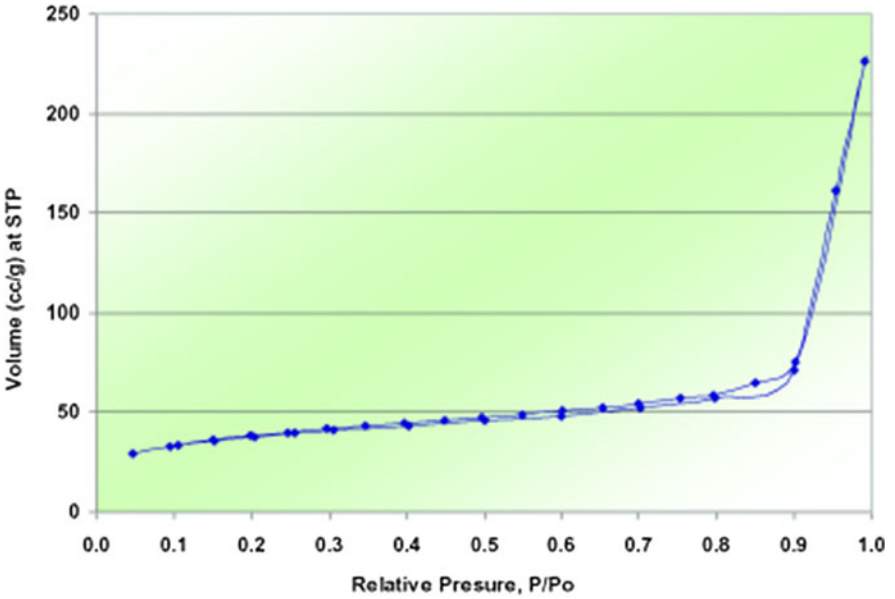

FIG. 7. N_2 adsorption desorption isotherms for rutile nanoparticles after 72 h of aging.

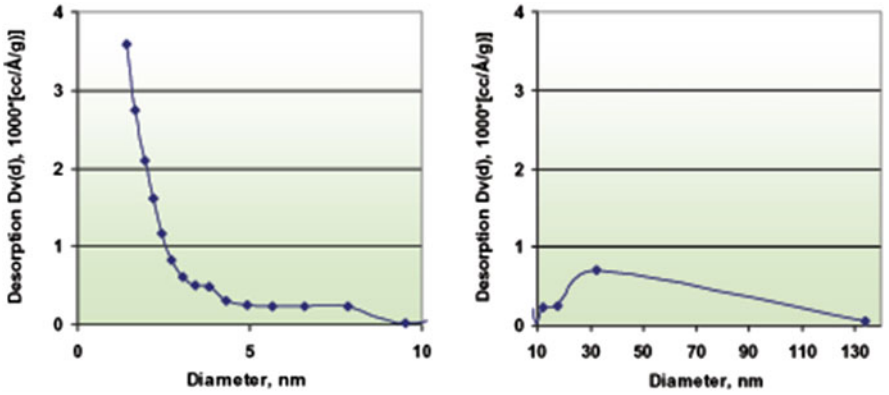

FIG. 8. Pore size distribution of rutile nanoparticles (72 h aged) determined from the N_2 desorption isotherm using the BJH method.

F. Postulations on the mechanism of crystal growth of rutile nanoparticles

When TTIP was added in distilled water, hydrolysis reaction proceeded fast leading to the formation of amorphous $Ti(OH)_4$ by the following reaction[16,25]:

$$Ti(C_3H_7O)_4 + 4H_2O \rightarrow Ti(OH)_4 + 4C_3H_7OH \quad \text{Hydrolysis} \quad , \qquad (2)$$

$$Ti(OH)_4 \rightarrow TiO_2 + 2H_2O \quad \text{Condensation} \quad . \qquad (3)$$

In the present study, from the observation it is assumed that the amorphous titania is dissolved to a transparent titania gel in stirred acidic solutions, and reprecipitated during the aging time over 72 h at room temperature. The reprecipitated particles are identified as crystalline particles by XRD and TEM.

According to Yin et al.,[15] the crystallization of titania proceeds from the reprecipitation from transparent solution of hydrated ion $[Ti(H_2O)6]^{4+}$. Before reprecipitation, titanium does not exist in the form of Ti^{4+} cation but exist as a sixfold coordinated hydrated ion $[Ti(H_2O)6]^{4+}$. These hydrated ions are dehydrated and polymerized to $[(H_2O)_4Ti–(OH)_2–Ti(H_2O)_4]^{6+}$, $[(H_2O)4TiO_2\ Ti(H_2O)_4]^{4+}$, and finally TiO_6 octahedra. It might be suggested that thermodynamically stable rutile nucleus with compact texture is formed by very slow precipitation rate at low temperatures. In this case, the rearrangement of TiO_6 octahedra was realized slowly during a long period of time, and finally, the rutile phase with a compact texture was formed. Wang et al.[16] observed that the longer addition time not only increases the fraction of rutile crystals but also alters the particle morphology. Differing from the above-mentioned mechanism, we have found that the rutile phase starts to form from the beginning (within 4 h) of the reprecipitation starts (Fig. 2). At 72 h of aging, the nanoparticles are found to be as quite matured crystalline rutile nanoparticles (Fig. 3).

TABLE I. Specific surface area and porosity of rutile nanoparticles after 72 h of aging.

S_{BET}[a] (m^2/g)	V_p[b] (cc/g)	D_p[b] (nm)
132.2	0.34	1.4

[a]BET surface area (S_{BET})
[b]Pore volume (V_p) and average pore diameter (D_p) [BJH desorption].

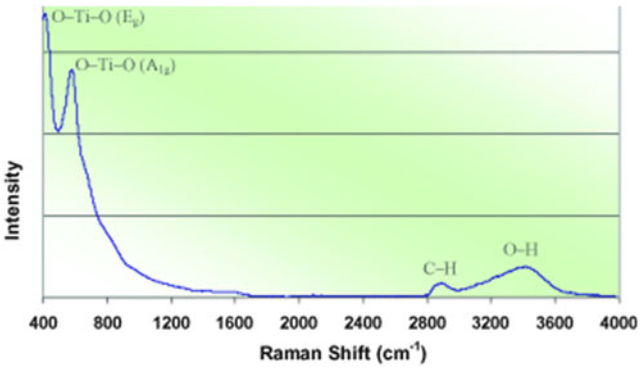

FIG. 9. Raman spectra of rutile nanoparticles after 72 h of aging.

TABLE II. Elemental analysis of rutile nanoparticles after 72 h of aging.

Elements	Carbon	Hydrogen	Nitrogen	Sulfur	Oxygen
% (wt/wt)	0.067	0.0729	0.000	0.000	5.372

The XRD data are quite consistent with that one obtained from HR-TEM data studies. The average grain size of rutile nanoparticles has been obtained as 11.3 nm by XRD. Again the rutile crystallite dimensions are 1.5–2.5 nm in diameter and 10–13 nm in length, whereas the dimensions of rutile nanoparticles are 25–30 nm in diameter and 130–150 nm in length. So it indicates that the crystallites are the building blocks for the formation of the self-organized nanoparticles. The crystal growth is

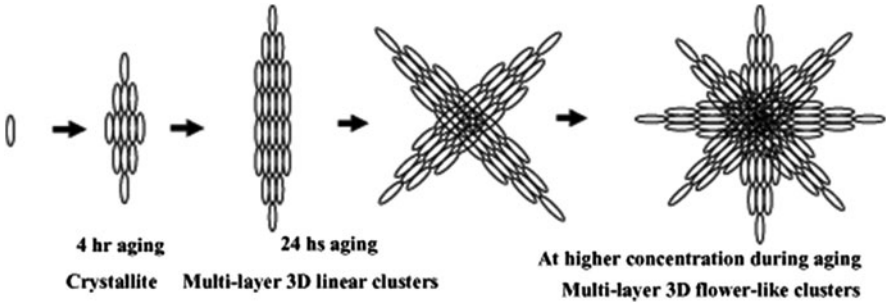

FIG. 10. Schematic representation of the formation of rutile nanoparticles.

TABLE III. Resistance (ρ), conductance (σ), and real part of relative permittivity (ε′) of the rutile nanoparticles.

Sample	ρ (Ω cm)	σ (S/cm)	ε′ at 10 MHz
Rutile	434476.0	2.3×10^{-6}	57

not continuous, i.e., the crystallites are arranged one after another and interconnected. Thereby the nanoparticles are microporous in nature by dint of intercrystallite voids. This postulation is well consistent with the HR-TEM and BJH porosity measurement data for the nanoparticles. The HR-TEM images also evaluate that some of the nanoparticles aggregate in an orderly fashion to give star-shaped or flower-shaped particles. In Fig. 10, the formation of self-organized rutile nanoparticles and ordered aggregation has been presented.

G. Electrical properties

Table III has been shown that the dielectric constant of rutile nanoparticles (72 h aged) has been found very high as 57 at 10 MHz AC frequency and DC conductance as 2.3×10^{-6} S/cm. This highly organized crystalline microporous metal-oxide semiconductor with high dielectric properties might suggest using for gas sensor applications.

IV. CONCLUSION

To the best of our knowledge, the LTDRP described here in harmony with Yin et al.[15] is the most economic route to synthesis of pure rutile nanoparticles. High yield (>80% at 3 days aging) and high specific surface area (>130 m^2/g) are the additional attractive features. Here, we have reported another very attractive feature of the rutile nanoparticles synthesized following that method: these nanoparticles are of highly self-organized crystalline microporous structure. We postulate that in conjunction with the luminescence property, this semiconductive (2.3×10^{-6} S/cm) and high dielectric constant (57 at 10 MHz) material with the large volume microporosity (average pore diameter, D_p = 1.4 nm; BJH desorption) and organized crystalline structure holds very good prospects for different applications.

ACKNOWLEDGMENT

The authors gratefully acknowledge the support from the Deanship of Graduate Research (DSR) program by King Saud University.

REFERENCES

1. M. Senna, N. Myers, A. Aimable, V. Laporte, C. Pulgarin, O. Baghriche, and P. Bowen: Modification of titania nanoparticles for photocatalytic antibacterial activity via a colloidal route with glycine and subsequent annealing. *J. Mater. Res.* **28**, 354 (2013).
2. J.M. Wu: Tin-doped rutile titanium dioxide nanowires: Luminescence, gas sensor, and field emission properties. *J. Nanosci. Nanotechnol.* **12**, 1434 (2012).
3. M.R. Karim, J.H. Yeum, M.S. Lee, and K.T. Lim: Preparation of conducting polyaniline/TiO_2 composite submicron-rods by the γ-radiolysis oxidative polymerization method. *React. Funct. Polym.* **68**, 1371 (2008).
4. J. Xu, C. Jia, B. Cao, and W.F. Zhang: Electrochemical properties of anatase TiO_2 nanotubes as an anode material for lithium-ion batteries. *Electrochim. Acta* **52**, 8044 (2007).
5. E. Baudrin, S. Cassaignon, M. Koelsch, J.P. Jolivet, L. Dupont, and J.M. Tarascon: Structural evolution during the reaction of Li with nano-sized rutile type TiO_2 at room temperature. *Electrochem. Commun.* **9**, 337 (2007).
6. S.L. Kim, S.R. Jang, R. Vittal, J. Lee, and K.J. Kim: Rutile TiO_2-modified multi-wall carbon nanotubes in TiO_2 film electrodes for dye-sensitized solar cells. *J. Appl. Electrochem.* **36**, 1433 (2006).
7. H.Y. Byun, R. Vittal, D.Y. Kim, and K.J. Kim: Beneficial role of cetyltrimethylammonium bromide in the enhancement of photovoltaic properties of dye-sensitized rutile TiO2 solar cells. *Langmuir* **20**, 6853 (2004).
8. M.R. Karim, K.T. Lim, M.S. Lee, K. Kim, and J.H. Yeum: Sulfonated polyaniline–titanium dioxide nanocomposites synthesized by one-pot UV-curable polymerization method. *Synth. Met.* **159**, 209 (2009).
9. M.R. Karim, H.W. Lee, I.W. Cheong, S.M. Park, W. Oh, and J.H. Yeum: Conducting polyaniline-titanium dioxide nanocomposites prepared by inverted emulsion polymerization. *Polym. Compos.* **31**, 83 (2010).
10. M. Kadoshima, M. Hiratani, Y. Shimamoto, K. Torii, H. Miki, S. Kimura, and T. Nabatame: Rutile-type TiO_2 thin film for high-*k* gate. *Thin Solid Films* **424**, 224 (2003).

11. N.D. Abazovic, M.I. Comor, M.D. Dramicanin, D.J. Jovanovic, S.P. Ahrenkiel, and J.M. Nedeljkovic: Photoluminescence of anatase and rutile TiO_2 particles. *J. Phys. Chem. B* **110**, 25366 (2006).
12. J.M. Wu, H.C. Shih, and W.T. Wu: Formation and photoluminescence of single-crystalline rutile TiO_2 nanowires synthesized by thermal evaporation. *Nanotechnology* **17**, 105 (2006).
13. Y. Zhu, J. Shi, Z. Zhang, C. Zhang, and X. Zhang: Development of a gas sensor utilizing chemiluminescence on nanosized titanium dioxide. *Anal. Chem.* **74**, 120 (2001).
14. T.P. Corrales, N.S. Allen, M. Edge, G. Sandoval, and F. Catalina: A chemiluminescence study of micron and nanoparticle titanium dioxide: Effect on the thermal stability of metallocene polyethylene. *J. Photochem. Photobiol., A* **156**, 151 (2003).
15. S. Yin, R. Li, Q. He, and T. Sato: Low temperature synthesis of nanosize rutile titania crystal in liquid media. *Mater. Chem. Phys.* **75**, 76 (2002).
16. L. Wang, Z. Yuan, and T.A. Egerton: The effects of different acids on the preparation of TiO_2 nanostructure in liquid media at low temperature. *Mater. Chem. Phys.* **133**, 304 (2012).
17. S.D. Park, Y.H. Cho, W.W. Kim, and S-J. Kim: Understanding of homogeneous spontaneous precipitation for monodispersed TiO_2 ultrafine powders with rutile phase around room temperature. *J. Solid State Chem.* **146**, 230 (1999).
18. J. Ovenstone: Preparation of novel titania photocatalysts with high activity. *J. Mater. Sci.* **36**, 1325 (2001).
19. A. Navrotsky and O.J. Kleppa: Enthalpy of the anatase-rutile transformation. *J. Am. Ceram. Soc.* **50**, 626 (1967).
20. JCPDS—International Centre for Diffraction Data, 2003, PCPDFWIN v. 2.4.
21. H.P. Klug and L.E. Alexander: *X-ray Diffraction Procedures for Polycrystalline and Amorphous Materials* (Wiley, New York, 1954); 491 pp.
22. S.N. Danilchenko, O.G. Kukharenko, C. Moseke, I.Y. Protsenko, L.F. Sukhodub, and B. Sulkio-Cleff: Determination of the bone mineral crystallite size and lattice strain from diffraction line broadening. *Cryst. Res. Technol.* **37**, 1234 (2002).
23. S. Watson, D. Beydoun, J. Scott, and R. Amal: Preparation of nanosized crystalline TiO_2 particles at low temperature for photocatalysis. *J. Nanopart. Res.* **6**, 193 (2004).
24. S.P.S. Porto, P.A. Fleury, and T.C. Damen: Raman spectra of TiO_2, MgF_2, ZnF_2, FeF_2, and MnF_2. *Phys. Rev.* **154**, 522 (1967).
25. D.A.H. Hanaor and C.C. Sorrell: Review of the anatase to rutile phase transformation. *J. Mater. Sci.* **46**, 855 (2011).